

The Fitted q-Gaussian Function, from Voigt Profile to Kubo Lineshape

Original

The Fitted q-Gaussian Function, from Voigt Profile to Kubo Lineshape / Sparavigna, Amelia Carolina. - In: INTERNATIONAL JOURNAL OF SCIENCES. - ISSN 2305-3925. - ELETTRONICO. - 13:3(2024), pp. 1-16. [10.18483/ijSci.2750]

Availability:

This version is available at: 11583/2986504 since: 2024-03-03T08:59:16Z

Publisher:

Alkhaer Publications

Published

DOI:10.18483/ijSci.2750

Terms of use:

This article is made available under terms and conditions as specified in the corresponding bibliographic description in the repository

Publisher copyright

(Article begins on next page)

The Fitted q-Gaussian Function, from Voigt Profile to Kubo Lineshape

Amelia Carolina Sparavigna¹

¹Department of Applied Science and Technology, Polytechnic University of Turin, Italy

Abstract: Several previously discussed cases have shown that the q-Gaussian Tsallis functions can be used for fitting the bands of Raman spectra. Here, considering an article by Thibault et al., 2002, we can add the case of the Raman Q branch of carbon monoxide, for mixtures with Argon at different temperatures. In Thibault et al., a plot is available for the Q(5) line with a fitted Voigt function. A q-Gaussian Tsallis function can be used for fitting this line too. We will note that the fitted q-Gaussian has the wings which are not Lorentzian. At the same time, the wings are not Gaussian. Besides the use of q-Gaussians, a discussion will be proposed about the time correlation functions related to different line shapes (q-Gaussian, Egelstaff-Schofield, Kubo, BWF, Voigt, speed-dependent Voigt, Galatry, Rautian, HTP). Some of these line shapes have been proposed for the high-resolution spectroscopy of gases; however, their knowledge can be relevant also for the condensed matter spectroscopy.

Keywords: Raman Spectroscopy, q-Gaussian Tsallis Lines, Time Correlation Functions, WolframAlpha

Introduction

The Voigt functions, convolutions of Gaussian and Lorentzian functions, and the q-Gaussian Tsallis functions can be used as line shapes in Raman spectroscopy for the analysis of spectra (Sparavigna, 2023). The Voigtian convolution possesses a bell shape with a Gaussian kernel and wings (tails) which are of the Lorentzian form. According to Cope and Lovett, 1987, the asymptotic solution of Voigtian expansion has the leading term equal to $a_0 / \pi x^2$, where x is the variable. The Voigt functions, or their approximations as pseudo-Voigtian functions, which are linear combinations of Gaussian and Lorentzian profiles, are suggested for instance in Meier, 2005, because of their corresponding time correlation functions related to the fundamental mechanisms of Raman photonic emissions. Let us also note that the Voigt profiles are intermediate between the Lorentzian and Gaussian outlines. The reason of using the Voigt functions is therefore also motivated by the fact that "intermediate" profiles are usually displayed by the Raman spectral lines (Kirillov, 2004).

The q-Gaussian functions have intermediate profiles too. The q-Gaussians, also known as "Tsallis functions", are probability distributions derived from the Tsallis statistics (Tsallis, 1988, 1995, Hanel et al., 2009). The q-Gaussians are based on a generalized form of the exponential function (see discussion in Sparavigna, 2022), characterized by a continuous parameter q in the range $1 < q < 3$. As given by Umarov et al., 2008, the q-Gaussian is based on function $f(x) = C e_q(-\beta x^2)$, where $e_q(\cdot)$ is the q-exponential function and C a constant. The q-exponential has expression:

$$\exp_q(u) = [1 + (1 - q)u]^{1/(1-q)} \quad (1a)$$

The function $f(x)$ possesses a bell-shaped profile. In the case that we have the peak at position x_0 , the q-Gaussian is:

$$\begin{aligned} \text{q-Gaussian} &= C \exp_q(-\beta(x - x_0)^2) = \\ &C [1 - (1 - q)\beta(x - x_0)^2]^{1/(1-q)} \quad (1b) \end{aligned}$$

For q equal to 2, the q-Gaussian is the Cauchy-Lorentzian distribution (Naudts, 2009). For q close to 1, the q-Gaussian is a Gaussian. For the q -parameter between 1 and 2, the shape of the q-Gaussian function is intermediate between the Gaussian and the Lorentzian profiles.

The q-Gaussian functions can imitate the Voigt convolutions, but they are different functions, in particular for what is regarding the behavior of the wings. So let us stress once more that, as told by Townsend, 2008, the Voigt function "looks like Gaussian for small x (i.e., near line center), and like Lorentzian for large x (i.e., out in line wings)". We can also appreciate the same by observing the pseudo-Voigt function, which is generally used for approximating the Voigt function. Being the pseudo-Voigt the linear combination of Gaussian and Lorentzian functions, the wings must be necessarily Lorentzian and the kernel Gaussian-like. Consequently, if we use Voigt functions or pseudo-Voigt functions for fitting spectra, the wings of the Raman lines will be always described by a Lorentzian behavior. However, is this always the experimental case? That is, are we always observing Lorentzian wings for the Raman bands? To answer these questions, we started investigation in [ChemRxiv1](#). We observed that a generalization of the pseudo-Voigt functions obtained by means of a linear combination of two q-Gaussians can help us in describing the leading term of the line wings. In this



manner, we can quantitatively measure the wing power law as well as answering qualitatively whether it is Lorentzian or not. The q-Gaussians are therefore the proper solution for investigation. Actually, for the spectra previously considered (Sparavigna, 2023), the fitted functions are successfully in several cases, for instance graphite, [ChemRxiv2](#), anatase [ChemRxiv3](#), SERS spectra, [ChemRxiv4](#), and so on, [SSRN](#).

For what is regarding the physics of Voigt function, let us consider the convolution theorem. This theorem states that the Fourier transform of a convolution is the product of the Fourier transforms of the convoluted functions. It means that the two related phenomena must have probability distributions which are independent (see discussion in Sparavigna, 2023). In the case of the Voigt convolution, the two distributions are those that we can find discussed for photonic emission in Svelto, 1970. They are the exponential decay and the Gaussian time functions, so that a spectral Lorentzian function is generally assumed as describing the photonic emission (or the broadening due to photonic interactions with phonons), and a spectral Gaussian function is considered to represent the thermal effects (or the effect of instrumentation).

In the case of the q-Gaussian function, the physics of the q-parameter is in its ability to evaluate the power law of the wings, as previously discussed. Moreover, as recently shown in [ijSciences](#), 2024, properly fitted q-Gaussian functions can be also proposed for the Kubo lineshapes, which are the Fourier transforms of Kubo stochastic time-correlation functions. In this manner a q-Gaussian function, with its simple analytic expression, can be used as a substitute of Kubo lineshape, which is requiring a numerical Fourier transform calculation. The value of the q-parameter turns out to be related to the time scales of dynamics (fast q=2, mid q=1.4, and slow q=1). Then, besides its ability of evaluating the wing power law, the q-Gaussian is also providing an estimation of the process modulation.

Besides investigating the q-Gaussians for the Raman spectroscopy of condensed matter, here we start considering further Raman bands, such as those of the isolated lines of gases, to explore the behavior of the wings and the scale of modulation processes.

Convolution

As previously told, the Voigt profile is a convolution of a Lorentz distribution L and a Gaussian distribution G given by:

$$V(k; \sigma, \gamma) = \{G * L\}(k) = \int_{-\infty}^{\infty} G(k'; \sigma) L(k - k'; \gamma) dk'$$

where k , in spectroscopy, is representing the shift from the line center, and:

$$G(k; \sigma) = \frac{e^{-k^2/(2\sigma^2)}}{\sigma\sqrt{2\pi}}$$

$$L(k; \gamma) = \frac{\gamma}{\pi(k^2 + \gamma^2)}$$

The convolution theorem states that the Fourier transform of a convolution of two functions is the pointwise product of their Fourier transforms. Let us consider two functions $G(k), H(k)$ and their Fourier transforms $g(x), h(x)$. As in the case of the Voigt function, the convolution is:

$$R(k) = \{G * H\}(k) = \int_{-\infty}^{\infty} G(k') H(k - k') dk'$$

And according to the [convolution theorem](#):

$$F\{R(k)\}(x) = F\{\{G * H\}(k)\}(x) = F\{G(k)\}(x) \cdot F\{H(k)\}(x) = g(x) \cdot h(x)$$

Please consider that operator F indicates the Fourier transform.

Burke et al., 2019, in their introduction to radio astronomy, consider the convolution theorem “easily proven” and with “many practical applications” (Burke et al., 2019). For instance, the Fourier transform of the Voigt function is the pointwise product of the Fourier transforms of Gaussian and Lorentzian functions:

$$F\{G * L\}(x) = F\{G(k)\}(x) \cdot F\{L(k)\}(x) = g(x) \cdot l(x)$$

The Fourier transform of a Gaussian is a Gaussian, so that, in the [Wolfram formalism](#):

$$g(x) = F\{e^{-ak^2}\}(x) = \sqrt{\frac{\pi}{a}} e^{-\pi^2 x^2/a},$$

and in the case of the [Lorentzian function](#):

$$l(x) = F\left\{\frac{1}{\pi(k - k_0)^2 + (\Gamma/2)^2}\right\}(x) = \exp(-2\pi i x k_0 - \Gamma\pi|x|)$$

This is the characteristic function of the Cauchy distribution. If we put the center k_0 at zero:

$$l(x) = \exp(-\Gamma\pi|x|)$$

If we consider variable x as the time, we have that the Fourier transform of the Voigt function is proportional to the product:

$$F\{V(k)\}(t) \propto \exp(-\Gamma\pi|t|) \cdot \exp(-At^2)$$

that is an exponential decay over time and a Gaussian function.

Let us note that methods for the fast computation of Voigt Function are based on the Fourier transform too (Schreier, 1992, Mendenhall, 2007, see please also the discussion by Vogman, 2010).

The use of the convolution theorem has been also appreciated for the comparison of different algorithms to evaluate the Voigt function (Abousahl et al., 1997). The approach by Abousahl and coworkers is based on F^{-1} Fourier anti-transform, so that:

$$V(k) = \{G*L\}(k) = F^{-1}\{g(x) \cdot l(x)\}(k)$$

Convolution (literature)

Before considering the time correlation function corresponding to a q-Gaussian, let us further discuss for a while convolution and transfer function.

As already made in [ChemRxiv5](#), let us consider the words by Orazio Svelto, 1970, about the homogeneous broadening of the photonic emission. In the case that we have a dipole damped oscillator model, we can observe the spectral line of the spontaneous emission with a “natural” or “intrinsic” broadening. This homogeneous broadening produces a line profile described by a Lorentzian function. Svelto is also mentioning the photon-phonon interaction as generating homogeneous broadening and therefore a Lorentzian line shape too. An inhomogeneous broadening (such as those caused by Doppler effect and thermal effect) is giving a Gaussian line shape. However, in spectroscopy, the most observed case is that of an intermediate profile, given by the convolution of the resonance relative probability and the broadening function, because the natural band can be modified by several different mechanisms (Svelto, 1970).

We have mentioned the natural broadening giving a Lorentzian profile, the thermal broadening introducing a Gaussian profile, and the general intermediate profiles as the most commonly observed case. A consequence is that the Voigt profile, that is the convolution of Gaussian and Lorentzian functions, is generally used to simulate the intermediate case.

Voigt profile is also used in the case of the spin resonance lines. In solids, these lines “are broadened by a number of mechanisms” (Stoneham, 1972). “Some of these mechanisms give a Gaussian lineshape, such as dipolar broadening in concentrated crystals (Van Vleck, 1948) and strain broadening by dislocations (Stoneham, 1966, 1969). Other mechanisms lead to a Lorentzian lineshape, such as the relaxation broadening due to the finite lifetime of a state” (Stoneham, 1972, is referring to the analogous broadening mechanism that we find in

Svelto, 1970). According to Stoneham, “If the mechanisms which lead to Lorentzian and Gaussian broadening are *independent*, the lineshape is just the convolution of a Gaussian and a Lorentzian”. That is, a Voigt function.

“Alternatively, [we can] suppose that the line is scanned by a spectrophotometer with a Gaussian sensitivity function” (Tatum, 2022). Then, in this experimental framework, we have the convolution of the line with the instrumental function profile. Let us remember that “the general expression that takes account of all the instrumentally induced distortion of the true band shape can be called the instrument function” (Seshadri and Jones, 1963). It is also known as the “instrumental transfer function” (Merlen et al., 2017). As told by S.G. Rautian, 1958: “Each monochromatic component $\varphi(x)dx$ of the true radiation is replaced by the apparatus [instrument] function, as a result of which, at some arbitrary point x' , there is created an illumination (or current) $a(x'-x)\varphi(x)dx$. Other monochromatic components of the true distribution also make a corresponding contribution to the illumination at the point x' , and as a result the observed distribution $f(x')$ will be expressed by the following integral”:

$$f(x') = \int_{-\infty}^{+\infty} a(x'-x)\varphi(x)dx$$

In the integral we have function $a(x)$ that considers “distortions both in the optical and recording parts of the apparatus” (Rautian, 1958). In Rautian, 1958, we can find several different instrumental functions that can be convoluted with the true radiation. And the true radiation can be a convolution of different broadening mechanisms.

The Voigt convolution is based on Lorentzian and Gaussian profiles because the analysis starts from a Lorentzian damping model (natural radiation) with a weight which is a Gaussian one. Different approaches exist (Kirillov, 2004), so that the true radiation line can be assumed different from a Lorentzian function; moreover, the weight function can be different from a pure Gaussian function.

Neglecting the transfer function

In Merlen et al., 2017, researchers are telling that “If we do not take into account the instrumental transfer function that can be negligible in many cases (...), the total intensity of one phonon mode with a wavevector q_0 and a frequency $\omega(q_0)$, in a perfect crystal, is spread on a symmetric profile which is Lorentzian”. Merlen et al. are also discussing the presence of asymmetric peaks in the framework of the approach by Richter et al., 1981. In the case of investigating the first order region of the Raman

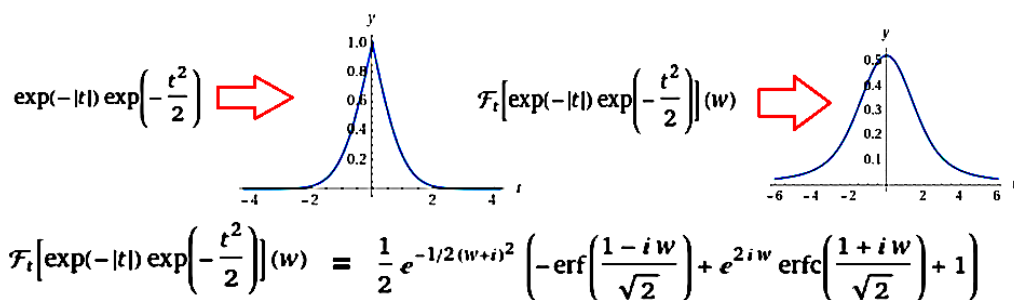
spectra of carbonaceous materials, for its fitting procedure, Merlen et al. suggest the use of Lorentzian and Gaussian functions for symmetric profiles and of the Breit-Wigner-Fano (BWF) line shape for asymmetric peaks.

In discussing the spectroscopy of carbonaceous materials, in particular G and G' bands, Merlen and coworkers tell the following. For “One band: The G band is fitted by a Lorentzian if symmetric, and by a BWF if not symmetric”. We have discussed G and G' bands of graphite in [ChemRxiv2](#) and we used q-Gaussians. We used q-Gaussians too for other carbonaceous materials (biochar and nanotubes) in [SSRN](#). The behavior of the peaks we considered is q-Gaussian, that is, not Lorentzian or Gaussian but q-Gaussian. For what is regarding the BWF asymmetric line shape, we started investigation about the [Raman LO mode band](#) in Silicon Carbide.

WolframAlpha approach

“The physical argument employed in establishing the Voigt profile is that the effects of Doppler and collision broadening are decoupled. Thus we argue that every point on a collision-broadened lineshape is further broadened by Doppler effects” (Ronald K. Hanson, 2018). Hanson is mentioning refinements with Galatry profiles (collision narrowing) and Berman profiles (speed-dependent broadening).

Before the discussion of refinements of the Voigt profile, let us consider software WolframAlpha to visualize the behavior of a Voigtian time correlation function, that is the product of exponential decay and Gaussian time functions. This product is producing, by means of its Fourier transform, a spectral Voigt convolution. Software is providing the plot of the function and its Fourier transform, as in the following example.



where erf is the error function and erfc the complementary error function.

q-Gaussians and Bessel functions

For what is regarding the q-Gaussian function and its Fourier transform, we need to tell that the specific formulation of the transform is quite complex (Rodrigues & Giraldi, 2015). However, we can find that the Fourier transform of q-Gaussian contains the K functions (modified Bessel function of the second kind). Here, let us consider (1) in the following form, with dimensionless variable w about w₀ = 0:

$$q\text{-Gaussian} = C \exp_q(-w^2) = C [1 - (1 - q)w^2]^{1/(1-q)} \quad (2)$$

and search for the Fourier transform of it, remembering that the Fourier transform of a Lorentzian line shape is producing a time correlation function which is an exponential decay over time, and that, in the case of the Gaussian line shape, we have a correlation with is a Gaussian function of time. Being the q-Gaussian a line shape which is intermediate between Lorentzian and Gaussian profiles, the related time correlation function must be

intermediate between the exponential decay over time and a Gaussian function.

As previously told, Rodrigues and Giraldi, 2015, have considered in detail the Fourier transform of q-Gaussian functions. Here we use a more phenomenological approach. Let us start from the link between the q-Gaussians and the Bessel functions.

In [Wikipedia](#) we find that the “Bessel functions can be described as Fourier transforms of powers of quadratic functions”. Function K_v is a modified Bessel function of the second kind, order v. For instance:

$$2 K_0(\omega) = \int_{-\infty}^{\infty} \frac{e^{i\omega t}}{\sqrt{t^2 + 1}} dt.$$

To have further cases, we can use the Fourier transform calculator by [WolframAlpha](#). Following the notation in Wikipedia, we can find, for instance:

$$\frac{1}{\sqrt{2\pi}} \int_{-\infty}^{\infty} (1 + (At)^2)^{-1/2} e^{iwt} dt = \frac{1}{\sqrt{A^2}} \cdot \sqrt{\frac{2}{\pi}} \cdot K_0\left(\frac{|w|}{\sqrt{A^2}}\right)$$

The Fourier transform (WolframAlpha) of the function with exponent $-1/(q-1)$, that is $1/(1-q)$ as in (2), from the frequency domain w to the time domain t (dimensionless variables) is given as follows:

Note that, in this example, we can see evidenced the time/frequency scaling, by using A factor.

$$F_w[(1 + w^2)^{-1/(q-1)}](t) = \frac{1}{\Gamma(\frac{1}{q-1})} \cdot 2^{\frac{q-2}{q-1}} \cdot |t|^{\frac{1}{q-1} - \frac{1}{2}} \cdot K_{\frac{1}{q-1} - \frac{1}{2}}(t \operatorname{sgn}(t))$$

Posing $\xi = 1/(q-1)$: $F_w[(1 + w^2)^{-\xi}](t) = \frac{1}{\Gamma(\xi)} \cdot 2^{(q-2)\xi} \cdot |t|^{\xi - \frac{1}{2}} \cdot K_{\xi - \frac{1}{2}}(t \operatorname{sgn}(t))$

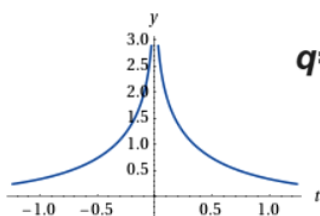
To illustrate the behavior of the Fourier transform, let us consider different values of q , starting from $q=3$, including $q=2$ (Lorentzian), to find the corresponding time correlations.

Fourier transform in the case $q=3$ (plot courtesy WolframAlpha)

From WolframAlpha, we have:

$$F_w[(1 + w^2)^{-1/(3-1)}](t) = \sqrt{\frac{2}{\pi}} K_0(t \operatorname{sgn}(t))$$

By the way, the q -Gaussian is defined for q ranging from 1 to 3.



$$F_w[(1 + w^2)^{-1/(2.5-1)}](t) = 0.930437 \cdot |t|^{0.166667} \cdot K_{0.166667}(t \operatorname{sgn}(t))$$

$$F_w[(1 + w^2)^{-1/(2-1)}](t) = \sqrt{\frac{\pi}{2}} e^{-|t|} \quad (a)$$

(Fourier transform of the Lorentzian function). In (a) we can find the Laplace distribution, that is the exponential decay over time.

$$F_w[(1 + w^2)^{-1/(1.9999-1)}](t) = 0.999988 \cdot |t|^{0.5001} \cdot K_{0.5001}(t \operatorname{sgn}(t)) \quad (a')$$

We can deduce that the exponential decay is equal to a K Bessel function multiplied by a square root, so that:

$$K_{0.5}(t \operatorname{sgn}(t)) = \sqrt{\frac{\pi}{2}} \frac{1}{\sqrt{|t|}} e^{-|t|}.$$

$$F_w[(1 + w^2)^{-1/(1.9-1)}](t) = 0.977728 \cdot |t|^{0.611111} \cdot K_{0.611111}(t \operatorname{sgn}(t)) \quad (b)$$

$$F_w[(1 + w^2)^{-1/(1.7-1)}](t) = 0.838525 \cdot |t|^{0.928571} \cdot K_{0.928571}(t \operatorname{sgn}(t)) \quad (c)$$

$$F_w[(1 + w^2)^{-1/(1.5-1)}](t) = \frac{0.626657}{t^2} \cdot e^{-|t|} \cdot |t|^2 \cdot (|t| + 1) = 0.626657 \cdot e^{-|t|} \cdot (|t| + 1) \quad (d)$$

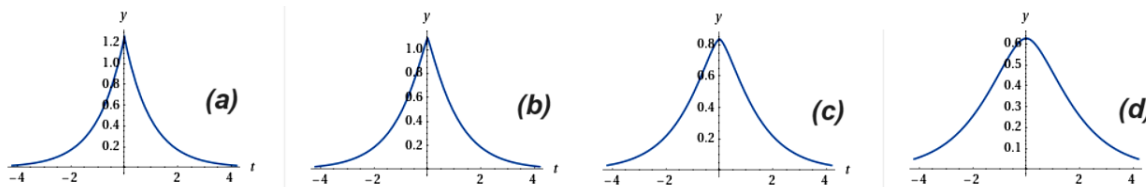
$$F_w[(1 + w^2)^{-1/(1.4999-1)}](t) = 0.499777 \cdot |t|^{1.5} \cdot K_{1.5}(t \operatorname{sgn}(t))$$

We have, as given by WoframAlpha, that: $K_{1.5}(t) = \frac{1.253314137}{\sqrt{t}} \cdot e^{(-t)} \cdot (\frac{1}{t} + 1)$, and therefore (d).

$$F_w[(1 + w^2)^{-1/(1.4-1)}](t) = 0.265962 \cdot |t|^2 \cdot K_2(t \operatorname{sgn}(t))$$

$$F_w[(1 + w^2)^{-1/(1.3-1)}](t) = 0.0714233 \cdot |t|^{2.83333} \cdot K_{2.83333}(t \operatorname{sgn} t)$$

$$F_w[(1 + w^2)^{-1/(1.15-1)}](t) = 0.000050 \cdot |t|^{6.16667} \cdot K_{6.16667}(t \operatorname{sgn} t)$$



Fourier transforms of four cases given above (plots courtesy WolframAlpha).

Let us add some further results, obtained by means of WolframAlpha.

$$F_w[(1 + w^2)^{-1/(1.25-1)}](t) = \frac{A}{t^4 \operatorname{sgn}(t)^4} |t|^{3.5} e^{-t \operatorname{sgn}(t)} \sqrt{t \operatorname{sgn}(t)}$$

$$A = (0.0261107 t^3 \operatorname{sgn}(t)^3 + 0.156664 t^2 \operatorname{sgn}(t)^2 + 0.391661 t \operatorname{sgn}(t) + 0.391661)$$

$$F_w[(1 + w^2)^{-1/(1.2-1)}](t) = \frac{A'}{t^5 \operatorname{sgn}(t)^5} |t|^{4.5} e^{-t \operatorname{sgn}(t)} \sqrt{t \operatorname{sgn}(t)}$$

$$A' = (0.00326384 t^4 \operatorname{sgn}(t)^4 + 0.0326384 t^3 \operatorname{sgn}(t)^3 + 0.146873 t^2 \operatorname{sgn}(t)^2 + 0.342703 t \operatorname{sgn}(t) + 0.342703)$$

And also:

$$\begin{aligned} \mathcal{F}_w[(1 + w^2)^{-1/(1.125-1)}](t) = & \\ \frac{1}{t^8 \operatorname{sgn}(t)^8} |t|^{7.5} e^{-t \operatorname{sgn}(t)} \sqrt{t \operatorname{sgn}(t)} & (1.94276 \times 10^{-6} t^7 \operatorname{sgn}(t)^7 + \\ & 0.0000543973 t^6 \operatorname{sgn}(t)^6 + 0.000734364 t^5 \operatorname{sgn}(t)^5 + 0.0061197 t^4 \operatorname{sgn}(t)^4 + \\ & 0.0336583 t^3 \operatorname{sgn}(t)^3 + 0.12117 t^2 \operatorname{sgn}(t)^2 + 0.262535 t \operatorname{sgn}(t) + 0.262535) \end{aligned}$$

Using the results given above and considering the scaling $(q - 1)w^2$ into $t/\sqrt{(q - 1)}$, we can plot some time correlations as in the Figure 1 (linear and semi logarithmic scales).

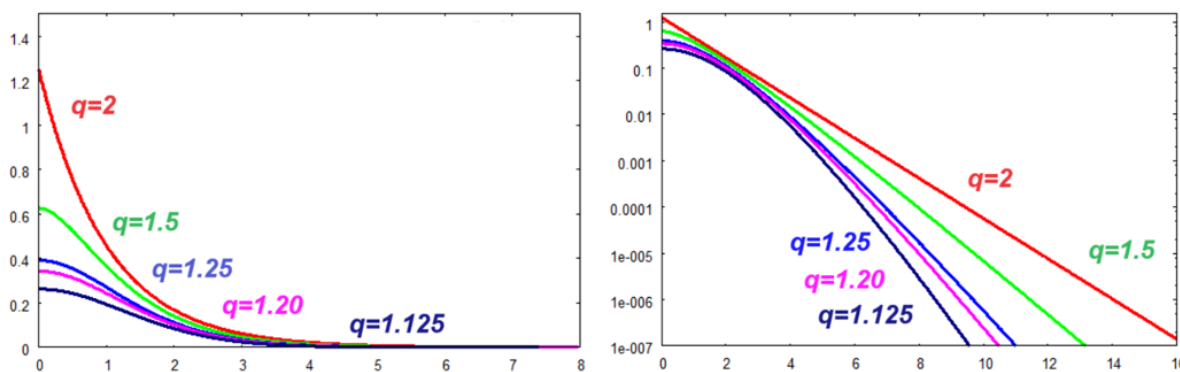


Figure 1: Left: Fourier transforms of q-Gaussians as given by WolframAlpha, for some values of the q parameter. Right: The same, in semi-logarithmic scale. For q=2, we have a time correlation which is an exponential decay function (straight red line). For q closer to 1, the curve is Gaussian-like (parabolic behavior in the semi-log plot).

In [Wikipedia](https://en.wikipedia.org/wiki/Sargan_distribution) we can find mentioned the Sargan distributions, given in the following form:

$$f_p(x) = \frac{1}{2} \exp(-\alpha|x|) \frac{1 + \sum_{j=1}^p \beta_j \alpha^j |x|^j}{1 + \sum_{j=1}^p j! \beta_j}$$

Note the presence of the exponential decay.

In the functions given above, we can find suggested the Sargan distributions indeed.

As told by Kotz and coworkers (2001), for modified Bessel functions, with order “ $\lambda = r + 1/2$, where r is a non-negative integer, the Bessel function K_λ has the closed form”:

$$K_{r+1/2}(u) = \sqrt{\frac{\pi}{2u}} e^{-u} \sum_{k=0}^r \frac{(r+k)!}{(r-k)!k!} (2u)^{-k} \tag{*}$$

This is formula A.0.10 in Kotz et al., 2001. For $r = 0$, we have (A.0.11):

$$K_{1/2}(u) = \sqrt{\frac{\pi}{2u}} e^{-u}$$

(see also the discussion at 4.4.3 in Kotz et al., 2001).

Let us consider again $K_{1.5}(t) = \frac{1.253314137}{\sqrt{t}} \cdot e^{-t} \cdot (\frac{1}{t} + 1)$, for instance. It is easy to find that this expression agrees with (*).

For further discussion, see Appendix.

We have not to be surprised to find time correlations containing Bessel functions. For instance, in Hall and Helfand, 1982, we can find them in time-correlation functions of the conformational state relaxation in polymers. Hall and Helfand studied the “relaxation processes in polymer molecules which proceed via conformational transitions of the chain backbone

from one rotational isomeric state to another. ... The resulting correlation functions contain a modified Bessel function which is associated with the diffusional nature of the process. This functional form has recently proven useful in fitting time-correlation functions determined in polymer simulations, which indicates that it will be of value in fitting data obtained in relaxation experiments on polymers” (Hall & Helfand, 1982).

Egelstaff-Schofield lineshape

With the aim of formulating the Fourier transform of the q-Gaussian function in a simpler manner (that is, to have a simpler function for the time correlation), in a [previous article](#) we discussed the Egelstaff-Schofield (ES) line shapes and the related fitted q-Gaussians. In fact, the ES profiles can be imitated by the q-Gaussians.

Let us stress that the ES profiles can be Fourier transformed into a simple analytical expression (Kirillov, 1999):

$$\Phi(t) = \exp\{-[(t^2 + \tau_1^2)^{1/2} - \tau_1]/\tau_2\}$$

According to Kirillov, 1999, this function becomes Gaussian for $t \ll \tau_1$, and decaying exponential for $t \gg \tau_1$.

Let us write the expression previously given as:

$$\Phi(t) = \exp\{-[(t^2 + a^2)^{1/2} - a]/b\}$$

The following plot is giving the behavior of this function.

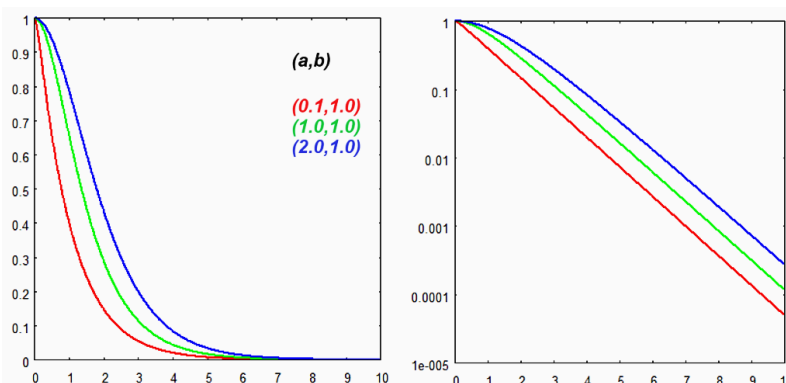
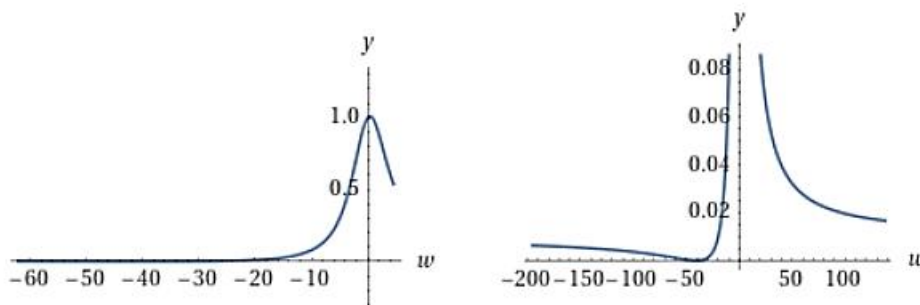


Fig.2: Behavior of the Egelstaff-Schofield time correlation. From the semi log scale, we can appreciate the deviation from the exponential decay (red line) at short times.

Breit-Wigner-Fano lineshape

Since we have mentioned it before, let us consider how can we express the time correlation function related to the Breit-Wigner-Fano line shape.

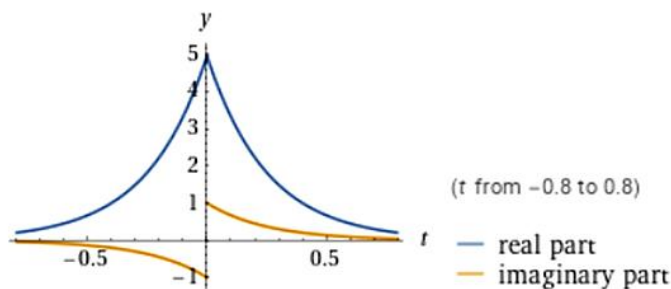
Let us consider it as defined in [Origin](#), with the same parameters. In WolframAlpha, let us use the input written as $(1+w/40)^2/(1+(w/4)^2)$, we have plots:



Plots courtesy WolframAlpha for the input given above.

The Fourier transform (Wolfram Alpha) is given as:

$$\mathcal{F}_w \left[\frac{\left(1 + \frac{w}{40}\right)^2}{1 + \left(\frac{w}{4}\right)^2} \right] (t) = \frac{1}{50} \sqrt{\frac{\pi}{2}} \delta(t) + \frac{1}{25} \sqrt{\frac{\pi}{2}} e^{-4t} \left((99 - 20i) e^{8t} \theta(-t) + (99 + 20i) \theta(t) \right)$$



Plot of the BWF Fourier transform (courtesy WolframAlpha).

In the case that $t > 0$, the Fourier transform reduces to: $(99/25 + 4i/5) \sqrt{\frac{\pi}{2}} e^{-4t}$. In general, for input $(q+w)^2/(1+w^2)$, that is $\frac{(q+w)^2}{(1+w^2)}$ as in Misochko and Lebedev, 2015, we find (WolframAlpha):

$$\sqrt{2\pi} \delta(t) + \sqrt{\frac{\pi}{2}} (q^2 - 1) e^{-t} (e^{2t} \theta(-t) + \theta(t)) - i \sqrt{2\pi} q e^{-t} (e^{2t} \theta(-t) - \theta(t))$$

This is the expression given for q and t real. In the case $t > 0$, it remains the exponential decay.

Beyond the Voigt profile

Besides the behavior of the wings, a relevant problem for the use of Voigt functions needs to be noted. To evaluate these functions, it is required a numerical approach because the convolution is an integral which cannot be solved analytically. The result is consequently depending on the model representing the convolution and, also, on the language used to implement the calculus and the related compiler required to obtain the numerical results. Some could claim that, today, due to the speed of computers we have no problems in any numerical calculus, however the problem of the used models remains,

because it has nothing to do with the speed of the calculus.

About the experimental data used for fitting, we must further consider that the raw signals have been processed by instrumentation and related software, before being proposed to the user as “raw” data for further processing. As previously told, the “transfer function” exists. We can guess it is negligible, but it could be not so.

Forthomme et al., 2015, asserted that the “Voigt profile (VP) is the standard lineshape model used in high resolution spectroscopy databases for its simplicity and its fast computation time”.

An example of database is HITRAN (high-resolution transmission molecular absorption database) which contains a compilation of molecular spectroscopic parameters. It “is used by various computer codes to predict and simulate the transmission and emission of light in gaseous media (with an emphasis on terrestrial and planetary atmospheres)” (Gordon et al., 2022).

However, as observed in Forthomme et al., 2015, “with the ever-increasing sensitivity and accuracy of measurement techniques, more subtle effects on the experimental data are now commonly observed”. Therefore, the Voigt profile needs to be revised. At low to moderate pressures, the “attempts to model measured lineshapes with a VP typically leaves a “w” shaped residual” (Forthomme et al., 2015). This difference is “associated with the narrowing that is not represented in the VP” (Forthomme et al. are mentioning the book by Hartmann et al., 2008). Let us note that the “w” shape residual is produced also by the fact that the wings of Voigt functions are Lorentzian. In our previously investigated cases, Sparavigna, 2023, the wings of the spectrum are not Lorentzian. Therefore, we can consider further lines from Raman spectroscopy, such as those of the isolated lines of gases, to evaluate the behavior of the wings by means of a q-Gaussian power law.

“A wide variety of models of various degrees of complexity have been proposed” to investigate spectral lines and to consider deviations from the Voigt profile: Forthomme and coworkers used the Hartmann-Tran profile. Besides this profile, we can find as quite popular the Rautian and Galatry symmetric profiles, and the asymmetric speed-dependent Voigt profile (Ivanov et al., 2014). The use of the Hartmann-Tran profile (HTP) was recommended in a IUPAC technical report regarding the “*line profiles of isolated high-resolution rotational-vibrational transitions perturbed by neutral gas-phase molecules*” (Tennyson et al., 2014). Tennyson and coworkers are stressing that the Voigt profile has “well-documented inadequacies” (no references are given, and inadequacies not mentioned at all). We can find told that HT profile “can be computed in a straightforward and rapid manner, and reduces to simpler profiles, including the Voigt profile, under certain simplifying assumptions”.

The HT profile is given in Eqs. (5),(6),(7) in [arXiv](#), and it contains seven parameters. According to Table II, the HT profile can be reduced to Voigt, Rautian, speed-dependent Voigt and speed-dependent Rautian functions. Let us stress, however, that we must calculate the complex Voigt integrals (with error

function, see Eq. 6 in the arXiv article) by numerical methods and therefore we need to refer to some related models. Voigt and complex error functions and related computational methods have been discussed by Schreier, 1992.

The Q(5) line

Being the Tsallis q-Gaussian function characterized by three parameters C, β and q , instead of comparing it with HTP (seven parameters when normalized to unit area), let us consider the Voigt function. We do comparison to understand the behavior of the spectral line wings for gases. Let us start from a Raman line in the Q branch of the carbon monoxide in mixture with Argon, that we can find in an article by Thibault et al., 2002. A plot is available for the Q(5) line and its fitted Voigt function. Here, in the following Figure 3, we show that a q-Gaussian Tsallis function can be fitted onto data recovered from Thibault et al.

From the Figure 3 we can note that the wings are not Lorentzian. The q parameter is equal to 1.87 (left). This means that the Raman lines of gases are interesting for further research about the power law of line wings.

Thibault and coworkers tell that the “spectral lines were individually fitted to the Voigt profile and the hard collision model profile of Rautian and Sobel’man. Since the collisional width determined from both models was within the error bars of the fitted parameter, [Thibault and coworkers] used only the Voigt profile for all measured lines. Figure 1 [in Thibault et al.] shows, as an example, the Q(5) line at 195 K and total pressure of 123.8 mbar for a 3% CO/Ar mixture spectrum. From the observed fitted residuals, it can be seen that the Voigt model fits the observed profile to within the noise”. Being within the noise, the Voigt line is proper for fitting.

The difference between the data recovered from Fig.1 in Thibault et al. and fitted q-Gaussian, shown in the lower part of the Figure 3, is of about plus/minus 1%. According to the Figure 1 of Thibault et al., 2002, the Voigt function is giving a difference of about plus/minus 3%. Our fitted q-Gaussian seems being able of giving even better results than the fitted Voigt function.

In the Figure 3 here proposed, data and q-Gaussians are given as functions of integers n (equally spaced points used in fitting), for the x -axis which is representing the Raman shift. A convenient scale is used for the y -axis (intensity axis). The fitting calculation is obtained by minimizing the sum of the squares of the deviations (sum from $n=1$ to $n=270$).

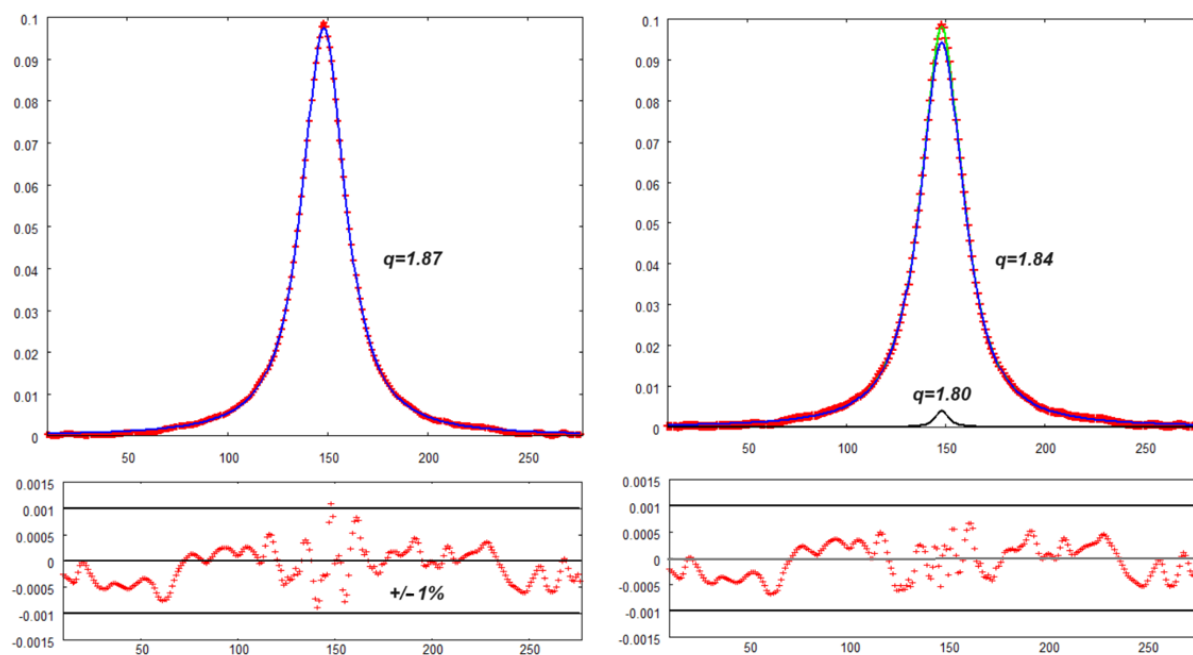


Fig.3: Left - The $Q(5)$ Raman line of the carbon monoxide as given in the Figure 1 of the article by Thibault et al., 2002, is here proposed with red points. The peak is at about 2142.75 cm^{-1} . The blue line is its fitted q -Gaussian. The q parameter of this function is equal to 1.87. In the lower part of the figure, the difference between data and q -Gaussian function is given. Note please that the difference is oscillating between plus/minus 1%. Right - The green line is representing the fitted linear combination of two q -Gaussians. The q parameter of the main component (blue) is equal to 1.84. In the lower part of the figure, the difference between data and two- q -Gaussians combination is given. Note please that the difference is oscillating between plus/minus 0.65%.

Let us stress that our “data” are the intensity values that we can obtain from the Figure 1 of Thibault et al., 2002, interpolated to have the red dots shows in our Figure 3.

Fitted q -Gaussian seems being better than fitted Voigt function, because of a lower misfit. But we must remark that our “data” are not the original point values obtained by Thibault and coworkers. Therefore, any further specific comparison could be questionable.

The Voigt function is usually approximated by a linear combination of a Lorentzian and a Gaussian function. This linear combination is known as the pseudo-Voigt. Here we can try to fit the peak in the Figure 3 (right) with a linear combination of two q -Gaussians. Is the fit in Figure 3 (right) better than that given in the Fig.3 (left)? In the Figure 3 (right) the misfit is lower, however both fits seem being within the “noise” band as depicted in the figures, and therefore we cannot assert that the fitted line in Fig.3 (right) is better than the fitted line in Figure 3 (left). In any case, the value of q of the main component changed just of 1.5%.

Discussion

Tennyson and coworkers tell that the “spontaneous emission of radiation is responsible for the natural lifetime broadening or intrinsic line width. This

component of the overall line shape is described by a Lorentzian profile which is, however, sufficiently narrow to be safely neglected in favour, ...” of two contributions which are the Doppler effect and the collisional broadening. The “well-known Doppler effect” has a profile (Doppler profile, DP), which is “expressed in terms of the Doppler half-width, Γ_D , by a Gaussian function” (Tennyson et al., 2014). The collisional broadening is producing a Lorentzian profile. “At low pressures the Doppler effect dominates, and as the pressure increases the effects of collisions become increasingly important. As a first approximation to get the resulting line shape, the convolution of an inhomogeneous Doppler profile with a homogeneous Lorentzian profile is commonly used. It defines the so-called VP [Voigt profile], which contains Doppler and Lorentzian shapes as limiting cases.” (Tennyson et al., 2014). And also: “The standard three-parameter VP, as already mentioned above, is the simplest line shape accounting for the pressure and Doppler effects.” Let us stress once more that the wings of VP are always of Lorentzian type, and that VP is based on causes of broadening which are statistically independent.

In Thibault et al., 2002, a detailed discussion is given about the determination of the Lorentzian contribution in the fitted Voigt profile, to evaluate the collisional width. The researchers “fixed the Gaussian width in the Voigt profile to that

corresponding to the convolution of the expected Doppler width for every line and temperature, and a Gauss function of 0.0026 cm^{-1} FWHM [full width at half maximum] to account for the apparatus function. Then, the collisional width was obtained as the Lorentz width resulting from the fit” (Thibault et al., 2002). In our Figure 3 the wings are not Lorentzian, because the fitted q-Gaussians have q-parameters equal to 1.87 and 1.84. These values of q-parameters tell us that we are quite close to a Lorentzian wing, so the collisional effect is the most relevant one.

The apparatus

In Thibault et al. we find mentioned the role of the apparatus, given as Gaussian. When the VP approach is used, many researchers assume that the Gaussian in the convolution is coming from the apparatus, with the result of a pure Lorentzian profile for the photonic emission. However, other effects, such as the Doppler effect considered in Thibault et al., with Gaussian influences participate to the broadening. Moreover, the Dicke effect exists producing a narrowing of Doppler broadening. The Dicke Effect, that is the “collision narrowing”, is the following. In the case that the mean free path of an atom is quite smaller than the wavelength of the radiative transition, a narrowing of the line is produced. The atom is changing its speed and direction several times during photonic emission or absorption. In average on the different Doppler states, we find that the atomic line width is narrower than the Doppler width (Basu, 2007, Demtröder, 1982).

“Of course, the choice of an appropriate line shape function is not a purely theoretical exercise and must be guided by fits to high accuracy measurements, which also need to consider the appropriate instrumental line shape function” (Tennyson et al., 2014). About the instrumental function and its role in the choice of the line shape, no discussion is given by Tennyson and coworkers.

Doppler effect and q-Gaussians

The q-Gaussian Tsallis distribution has been proposed by Silva Jr et al., 1998, for being applied to the q-Doppler broadening of spectral lines. Silva Jr and coworkers discussed the Doppler effect “using the q-Maxwellian velocity distribution”. However, the q-Gaussian is a function which can be able of expressing not only the Doppler (inhomogeneous) limiting case, but also the (homogeneous) collisional limiting case. Therefore, the q-Gaussian profile needs to be considered in a more general framework.

Time correlation functions

In Rohart et al., the time correlation function of the Voigt model is given as:

$$\Phi = \exp \left[i\omega_0 t - \Gamma t - \left(\frac{kv_{a0}t}{2} \right)^2 \right]$$

or the product of two exponential functions:

$$\Phi = \exp[i\omega_0 t - \Gamma t] \cdot \exp \left[- \left(\frac{kv_{a0}t}{2} \right)^2 \right]$$

ω_0, Γ are the line center frequency and the collisional relaxation rate (given in s^{-1}). The wave number and the most probable value of the absorber speed are $k = \omega_0/c, v_{a0} = \sqrt{2k_B T/m_a}$. T is the temperature, k_B the Boltzmann constant and m_a the molecular mass of the absorber.

Beyond VP, we find in Ngo et al., 2013, mentioned the work by Boone et al., 2007, in relation to the speed-dependent Voigt (SDV) profile. This profile “is the real part of the Fourier transform of the polarization correlation function” as given by Rohart, et al., 2003. The modification of the Voigt function, shown by Rohart et al., maintains the exponential factor related to the Fourier transform of the Lorentzian function, but the Gaussian is substituted by two factors, one of which is containing an irrational function. As proposed in the Eq.9 by Rohart et al., 2003, and Eq.7 in 2008, we have:

$$\Phi = \exp\{i\omega_0 t - (\Gamma_0 - 3\Gamma_2/2)t\} \cdot \frac{1}{(1 + \Gamma_2 t)^{3/2}} \cdot \exp \left\{ \frac{-(kv_{a0}t)^2}{4(1 + \Gamma_2 t)} \right\} \quad (2)$$

where Γ_0, Γ_2 are the mean relaxation rate over molecular speeds, and the speed dependence of the relaxation rate. Rohart and coworkers are also mentioning the Galatry profile (the HTP has not it as limit case). So let us show what is the correlation function generating the Galatry profile:

$$\Phi = \exp[i\omega_0 t - \Gamma_0 t] \cdot \exp \left\{ \frac{1}{2} (k v_{a0}/B)^2 \cdot \{1 - Bt - \exp(-Bt)\} \right\} \quad (3)$$

where Γ, B are the relaxation rate and the optical diffusion rate. We can find the Galatry profile given also in Dore, 2003.

In Ivanov et al., 2014, the Voigt and the Rautian profiles are formulated in the following manner (see please the parameters x, y, z defined in the article by Ivanov et al.). The Voigt profile:

$$f_V(x, y) = \text{RealPart}[w(x, y)]$$

where

$$w(x, y) = \frac{1}{\pi} \int_{-\infty}^{\infty} \frac{\exp(-t^2)}{x + iy - t} dt$$

And the Rautian profile:

$$f_R(x, y, z) = \text{RealPart} \left[\frac{w(x, y + z)}{1 - \sqrt{\pi} \cdot z \cdot w(x, y + z)} \right]$$

For what is regarding the Rautian line shape, we can find it proposed in Rautian and Sobel'man, 1967. "A simultaneous account of radiative decay and the Doppler effect involves no difficulties, since these causes of broadening are statistically independent. As we know, the correlation function in this case equals the product of the correlation functions describing each of the causes of broadening individually". But Rautian and Sobel'man are also stressing that "broadening due to interaction and that due to the Doppler effect are statistically dependent in the general case. Broadening due to interactions involves a phase shift of the atomic oscillator when the atom collides with surrounding particles. Obviously, both the phase of the oscillations and the velocity of translational motion of the atom can be altered in the same collision."

The Rautian and Sobel'man correlation function is not proposed in the simple forms as in (2) and (3). This is also the case of the correlation giving HTP line shape. Let us add that the Lorentzian profile is not a lower-order line model of HTP, that is, the Lorentzian profile is not given in the Table II by Tennyson et al.

Caveats

Adkins and Hodges, 2019, in their "assessment of the precision, bias and numerical correlation of fitted parameters" obtained by means of the Hartmann-Tran profile, tell that IUPAC-recommended HTP "has emerged as a widely utilized spectroscopic model profile for high resolution spectroscopy with the caveat that its use requires high signal-to-noise ratio data, adequate constraints, and a wide pressure range". Adkins and Hodges also tell: "Many laboratories ... use custom software for conducting multi-spectrum HTP fits with known and unknown differences in how the line shape and other parameters are defined. Differences between models

used in the fitting and parameterization for spectroscopic databases can lead to incompatibility in line parameters and down-stream algorithms such that they cannot be used to reproduce fits to experimental data". Let us add that, if we need functions which are numerically calculated, we have also to know the numerical methods used to define them, that is, the used subroutines, and the compiler involved in calculations too.

The Kubo case

Kubo, in 1969, proposed a stochastic theory of line shapes. His Gaussian-Markovian approach, or Kubo approach, "remains the most common and widely used in spectroscopic practice" (Kirillov, 1999). Kirillov is referring to condensed matter spectroscopy. The correlation is given by (M_2 is the second spectral moment and τ_ω a relaxation time):

$$\Phi = \exp\{-M_2\tau_\omega^2[\exp(-t/\tau_\omega) - 1 + t/\tau_\omega]\}$$

that is

$$\Phi = \exp\{-M_2\tau_\omega t\} \cdot \exp\{M_2\tau_\omega^2[1 - \exp(-t/\tau_\omega)]\} \tag{4}$$

Here the frequency is referred to the position of the unshifted frequency. Note please once more that correlations (2) and (3), such as (4), have an exponential decaying factor, which is the Fourier transform of a Lorentzian function; that is, we have the line subjected to homogeneous broadening mechanisms. Let us also remember that, considering independent phenomena, they appear as factors in the correlations.

The Kubo case, in the Lecture Notes by Tokmakoff, 2009, is given as:

$$F = \exp[-\Delta^2\tau_c^2(\exp(-t/\tau_c) + t/\tau_c - 1)]$$

where τ_c is the time scale of dynamics. Parameter $\kappa = \Delta \cdot \tau_c$ is introduced, and three cases are given: fast, $\Delta = 1, \tau_c = 0.2, \kappa = 0.2$, mid, $\Delta = 1, \tau_c = 1, \kappa = 1$, and slow $\Delta = 1, \tau_c = 10, \kappa = 10$. The absorption lineshapes are given by Tokmakoff as in the following plot (Fig.4).

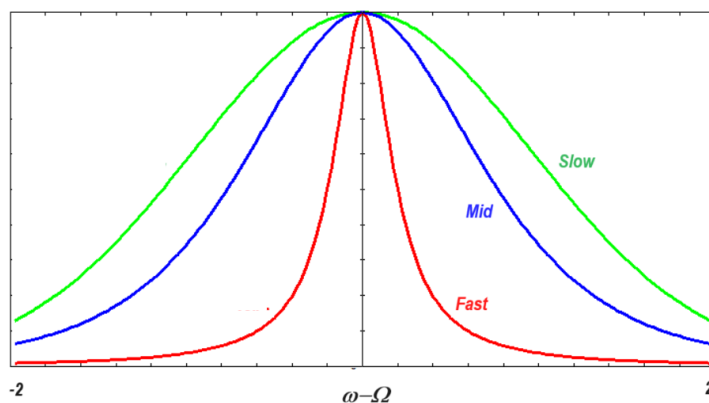


Fig.4.

“We see that for a fixed distribution of frequencies Δ the effect of increasing the time scale of fluctuations through this distribution (decreasing τ_c) is to gradually narrow the observed lineshape from a Gaussian distribution of static frequencies with width (FWHM [Full width at half maximum]) of $2.35 \cdot \Delta$ to a motionally narrowed Lorentzian lineshape with width (FWHM) of $\Delta \cdot \kappa/\pi$.” (Tokmakoff, 2009). Here again we are facing the problem to find the “intermediate” function between Lorentzian and Gaussian profiles.

Of this profile, we discussed in detail in the article “Kubo Lineshape and its Fitted q-Gaussian Tsallis Function”, in 2024 *ijSciences*. It has been shown that properly fitted q-Gaussian functions can be proposed for the Kubo lineshape, which is the Fourier transform of Kubo stochastic time-correlation function. As already told in the introduction, the value of the q-parameter turns out to be related to the time scale of dynamics (fast $q=2$, mid $q=1.4$ and slow $q=1$). The q-Gaussian can provide an estimation of the process modulation.

In Kirillov, 2004, it is told that “the Kubo TCF [time correlation function] corresponds to vibrational lines whose profiles vary from Gaussian to Lorentzian”.

In the analysis proposed in *ijSciences*, where we used fitted q-Gaussians to characterize the Kubo profile with the q-parameter, we concluded that the fast case has a q-parameter equal to 2 and the Kubo line shape is almost equal to a Lorentzian function. However, the slow case does not become a Gaussian profile. The result is shown in the following Figure 5. The difference is in the far wing.

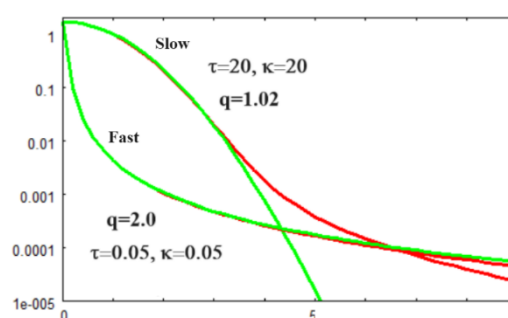


Fig. 5: Kubo line shapes in red and q-Gaussian in green. Being the line shape symmetric, only the right side is given in the semi-log plot.

The generalized Kubo case

As previously told, Kirillov, 1999, proposed a time correlation function corresponding to the Egelstaff-Schofield (ES) line shape. His aim was that of being able to manage the Rothschild-Kubo model (Rothschild et al., 1987, Feng and Wilde, 1988).

“Efforts to apply a simple Gauss-Markov theory have proven unsuccessful for aqueous ionic solutions, where strong Coulombic and dipolar forces promote vibrational relaxation, and the hydrogen bonding of the water inhibits anion reorientation. An alternate modeling function, the stretched exponential, has been proposed to explain inhomogeneously broadened Raman spectra” (Feng & Wilde, 1988). Feng and Wilde consider the “vibrational autocorrelation function $C(t)$, which is obtained by Fourier transforming the isotropic band”. $C(t)$ is given here as:

$$\Phi = \exp \left(i\omega_0 t - \int_0^t (1 - \tau) \chi(\tau) dt \right) ;$$

$$\chi(t) = M_2 \exp\{-(t/T)^\alpha\}$$

M_2 is the second spectral moment.

Rothschild et al., 1987, wrote this time correlation as:

$$\Phi = \exp\left(-M_2 T^2 \sum_{n=0}^{\infty} \frac{(-1)^n (t/T)^{2+n\alpha}}{n! (1+n\alpha)(2+n\alpha)}\right) \quad (5)$$

In fact, Rothschild and coworkers, in 1987, aimed to improve the Kubo model using the stretched exponentials. In Kirillov, 2004, we can find the Rothschild-Perrot-Guillaume (RPG) model as in Eq.(5), discussed with the Burshtein-Fedorenko-Pusep (BFP) model too.

"Differences in TCFs [time correlation functions] lead to very unlike line profiles. ... the Kubo TCF corresponds to vibrational lines whose profiles vary from Gaussian to Lorentzian" (Kirillov, 2004). However, it is better to remember that, in the case of slow modulation, the Kubo line is not precisely a Gaussian. "The Rothschild-Perrot-Guillaume TCF corresponds to vibrational lines of quite specific, over-Gaussian form. They are less sharp than Gaussian in their central part, and much faster fall to zero in the wings. The Burshtein, Fedorenko and Pusep TCF corresponds to over-Lorentzian line profiles. They are sharper than true Lorentzians in their central part, and broader in the wings" (Kirillov, 2004). In the cases of RPG and BFP lines, further research is required to grasp the meaning of "over-Gaussian" and "over-Lorentzian" behaviors.

To use (5) in spectroscopy, we need its Fourier transform to determine the corresponding line profile. Being the Fourier transform calculation too heavy for Raman bands deconvolution, Tagliaferro et al., 2020, have proposed a synthetic profile mimicking the lineshape. It is a profile named "GauLor", which is a piecewise symmetric function with a Lorentzian central part and wings which are Gaussians; actually, it seems being the opposite of the Voigt profile (Gaussian central part and Lorentzian wings). In GauLors, the onset of the wing happens at a frequency threshold, determined by the overall fitting approach. At the threshold, the Lorentzian and Gaussian piece functions and their derivatives are continuous. Supposing the existence of the threshold within the Raman scan range, the GauLor has the

References

1. Abousahl, S., Gourma, M., & Bickel, M. (1997). Fast Fourier transform for Voigt profile: comparison with some other algorithms. *Nuclear Instruments and Methods in Physics Research Section A: Accelerators, Spectrometers, Detectors and Associated Equipment*, 395(2), 231-236.
2. Adkins, E. M., & Hodges, J. T. (2022). Assessment of the precision, bias and numerical correlation of fitted parameters obtained by multi-spectrum fits of the Hartmann-Tran line profile to simulated absorption spectra. *Journal of Quantitative Spectroscopy and Radiative Transfer*, 280, 108100.
3. Basu, S. K. (Ed.). (2007). *Encyclopedic Dictionary of Astrophysics*. Global Vision Pub House.

onset of the Gaussian wing which can be very close to the center of the line (in the kernel) or quite far from it (in the far line wings). In fact, we have two families of intermediate functions between Lorentzian and Gaussian line shapes, and they are the q-Gaussians and the GauLors.

Further investigation is necessary about the generalization of the Kubo line shapes.

Appendix

In Yin and Dong, 2023, we can find the "Bessel function expression of characteristic function". The researchers are proposing a "unified method to derive the classical characteristic functions of all elliptical and related distributions in terms of Bessel functions". They are presenting "the simple closed form of characteristic functions for commonly used distributions such as multivariate t , Pearson Type II, Pearson Type VII, Kotz type and Bessel distributions", so we can enlarge the basin of functions which can be investigated by means of WolframAlpha. In fact, in Yin and Dong [arXiv](#), we can find the modified Bessel function of the second kind, with order ν , defined by the following WolframAlpha integral:

$$\sqrt{\frac{2}{\pi}} \int_0^{\infty} (1+w^2)^{-(\nu+1/2)} \cos(tw) dw = \frac{2^{1/2-\nu} |t^\nu| K_\nu(t \operatorname{sgn}(t))}{\Gamma(\nu+1/2)}$$

This is the Fourier transform that we can obtain by means of the WolframAlpha software of function:

$$(1+w^2)^{-(\nu+1/2)}$$

The expression of Pearson Type VII, is given in [Origin-Help](#) for instance, where it is told that the "peak function is a Lorentz function raised to a power". In this case too we can use WolframAlpha to obtain its Fourier transform and therefore its time correlation function.

4. Boone, C. D., Walker, K. A., & Bernath, P. F. (2007). Speed-dependent Voigt profile for water vapor in infrared remote sensing applications. *Journal of Quantitative Spectroscopy and Radiative Transfer*, 105(3), 525-532.
5. Burke, B. F., Graham-Smith, F., & Wilkinson, P. N. (2019). *An introduction to radio astronomy*. Cambridge University Press.
6. Cope, D., & Lovett, R. J. (1987). A general expression for the Voigt profile. *Journal of Quantitative Spectroscopy and Radiative Transfer*, 37(4), 377-389.
7. Demtröder, W. (1982). *Laser spectroscopy*. Berlin, Heidelberg: Springer.
8. Dicke, R. H. (1953). The effect of collisions upon the Doppler width of spectral lines. *Physical Review*, 89(2), 472.

9. Dore, L. (2003). Using Fast Fourier Transform to compute the line shape of frequency-modulated spectral profiles. *Journal of Molecular Spectroscopy*, 221(1), 93-98.
10. Egelstaff, P. A., & Schofield, P. (1962). On the evaluation of the thermal neutron scattering law. *Nuclear Science and Engineering*, 12(2), 260-270
11. Farvardin, N., & Modestino, J. W. (1984). Optimum quantizer performance for a class of non-Gaussian memoryless sources. *IEEE Trans. Inf. Theory*, vol. IT-30, no. 3, pp. 485-497, May 1984.
12. Feng, Q., & Wilde, R. E. (1988). Vibrational dephasing in aqueous KSCN solution. A memory function and stretched exponential study. *Chemical physics letters*, 150(6), 424-428.
13. Forthomme, D., Cich, M. J., Twagirayezu, S., Hall, G. E., & Sears, T. J. (2015). Application of the Hartmann-Tran profile to precise experimental data sets of 12C2H2. *Journal of Quantitative Spectroscopy and Radiative Transfer*, 165, 28-37.
14. Galatry, L. (1961). Simultaneous effect of Doppler and foreign gas broadening on spectral lines. *Physical Review*, 122(4), 1218.
15. Gordon, I. E., Rothman, L. S., Hargreaves, R. J., Hashemi, R., Karlovets, E. V., Skinner, F. M., Conway, E. K., Hill, C., Kochanov, R. V., Tan, Y., & Weislo, P. (2022). The HITRAN2020 molecular spectroscopic database. *Journal of quantitative spectroscopy and radiative transfer*, 277, p.107949.
16. Hall, C. K., & Helfand, E. (1982). Conformational state relaxation in polymers: Time-correlation functions. *The Journal of Chemical Physics*, 77(6), 3275-3282.
17. Hanel, R., Thurner, S., & Tsallis, C. (2009). Limit distributions of scale-invariant probabilistic models of correlated random variables with the q-Gaussian as an explicit example. *The European Physical Journal B*, 72(2), 263.
18. Hanson, R. K. (2018). Quantitative laser diagnostics for combustion chemistry and propulsion. [Archive](#).
19. Hartmann, J. M., Boulet, C., & Robert, D. (2008). Collisional effects on molecular spectra: Laboratory experiments and models, consequences for applications, Elsevier: Amsterdam, 2008.
20. Ivanov, S. V., Semenov, V. M., Nabiev, S. S., & Ponurovskii, Y. (2014). Diode laser measurements of the first overtone HF lineshape broadened by Ar, Xe, Kr and N2. *Applied Physics B*, 117, 423-435.
21. Kirillov, S. A. (1993). Markovian frequency modulation in liquids. Analytical description and comparison with the stretched exponential approach. *Chemical physics letters*, 202(6), 459-463.
22. Kirillov, S. A. (1999). Time-correlation functions from bandshape fits without Fourier transform. *Chemical physics letters*, 303(1-2), 37-42.
23. Kirillov, S. A. (2004). Novel approaches in spectroscopy of interparticle interactions. Raman line profiles and dynamics in liquids and glasses. *Journal of molecular liquids*, 110(1-3), 99-103.
24. Kirillov, S. (2004). Novel approaches in spectroscopy of interparticle interactions. Vibrational line profiles and anomalous non-coincidence effects. In *Novel Approaches to the Structure and Dynamics of Liquids: Experiments, Theories and Simulations*; Springer: Berlin/Heidelberg, Germany, 2004; pp. 193-227
25. Kotz, S., Kozubowski, T., & Podgórski, K. (2001). The Laplace distribution and generalizations: a revisit with applications to communications, economics, engineering, and finance (No. 183). Springer Science & Business Media. See also 4.4.3 in Kotz et al.
26. Kubo, R. (1969). A stochastic theory of line shape. *Advances in chemical physics*, 15, 101-127
27. Meier, R. J. (2005). On art and science in curve-fitting vibrational spectra. *Vibrational spectroscopy*, 2(39), 266-269.
28. Mendenhall, M. H. (2007). Fast computation of Voigt functions via Fourier transforms. *Journal of Quantitative Spectroscopy and Radiative Transfer*, 105(3), 519-524.
29. Merlen, A., Buijnsters, J. G., & Pardanaud, C. (2017). A guide to and review of the use of multiwavelength Raman spectroscopy for characterizing defective aromatic carbon solids: From graphene to amorphous carbons. *Coatings*, 7(10), 153.
30. Misochko, O. V., & Lebedev, M. V. (2015). Fano interference at the excitation of coherent phonons: Relation between the asymmetry parameter and the initial phase of coherent oscillations. *Journal of Experimental and Theoretical Physics*, 120, 651-663.
31. Naudts, J. (2009). The q-exponential family in statistical physics. *Central European Journal of Physics*, 7, 405-413.
32. Ngo, N. H., Lisak, D., Tran, H., & Hartmann, J. M. (2013). An isolated line-shape model to go beyond the Voigt profile in spectroscopic databases and radiative transfer codes. *Journal of Quantitative Spectroscopy and Radiative Transfer*, 129, 89-100.
33. Rautian, S. G. (1958). Real spectral apparatus. *Soviet Physics Uspekhi*, 1(2), 245.
34. Rautian, S. G., & Sobel'man, I. I. (1967). The effect of collisions on the Doppler broadening of spectral lines. *Soviet Physics Uspekhi*, 9(5), 701.
35. Richter, H., Wang, Z. P., & Ley, L. (1981). The one phonon Raman spectrum in microcrystalline silicon. *Solid State Communications*, 39(5), 625-629.
36. Rodrigues, P. S., & Giraldi, G. A. (2015). Theoretical Elements in Fourier Analysis of q-Gaussian Functions. *Theoretical and Applied Informatics*, 16-44.
37. Rohart, F., Colmont, J. M., Wlodarczak, G., & Bouanich, J. P. (2003). N2-and O2-broadening coefficients and profiles for millimeter lines of 14N2O. *Journal of Molecular Spectroscopy*, 222(2), 159-171.
38. Rohart, F., Wlodarczak, G., Colmont, J. M., Cazzoli, G., Dore, L., & Puzzarini, C. (2008). Galatry versus speed-dependent Voigt profiles for millimeter lines of O3 in collision with N2 and O2. *Journal of Molecular Spectroscopy*, 251(1-2), 282-292.
39. Rothschild, W. G., Perrot, M., & Guillaume, F. (1987). On the vibrational T 2 processes in partially ordered systems. *The Journal of chemical physics*, 87(12), 7293-7299.
40. Schreier, F. (1992). The Voigt and complex error function: A comparison of computational methods. *Journal of Quantitative Spectroscopy and Radiative Transfer*, 48(5-6), 743-762.
41. Seshadri, K., & Jones, R. N. (1963). The shapes and intensities of infrared absorption bands—A review. *Spectrochimica Acta*, 19(6), 1013-1085
42. Silva Jr, R., Plastino, A. R., & Lima, J. A. S. (1998). A Maxwellian path to the q-nonextensive velocity distribution function. *Physics Letters A*, 249(5-6), 401-408.
43. Sparavigna, A. C. (2022). Entropies and Logarithms. *Zenodo*. DOI 10.5281/zenodo.7007520
44. Sparavigna, A. C. (2023). q-Gaussian Tsallis Line Shapes and Raman Spectral Bands. *International Journal of Sciences*, 12(03), 27-40.
45. Sparavigna, A. C. (2023). q-Gaussian Tsallis Functions and Egelstaff-Schofield Spectral Line Shapes. *International Journal of Sciences*, 12(03), 47-50.
46. Sparavigna, A. C. (2023). q-Gaussian Tsallis Line Shapes for Raman Spectroscopy (June 7, 2023). SSRN Electronic Journal. <http://dx.doi.org/10.2139/ssrn.4445044>
47. Sparavigna, A. C. (2023). Tsallis and Kaniadakis Gaussian functions, applied to the analysis of Diamond Raman spectrum, and compared with Pseudo-Voigt functions. *Zenodo*. <https://doi.org/10.5281/zenodo.8087464>
48. Sparavigna A. C. (2023). Tsallis q-Gaussian function as fitting lineshape for Graphite Raman bands. *ChemRxiv*. Cambridge: Cambridge Open Engage; 2023.

49. Sparavigna A. C. (2003). Fitting q-Gaussians onto Anatase TiO₂ Raman Bands. ChemRxiv. Cambridge: Cambridge Open Engage; 2023.
50. Sparavigna, A. C. (2023). SERS Spectral Bands of L-Cysteine, Cysteamine and Homocysteine Fitted by Tsallis q-Gaussian Functions. International Journal of Sciences, 12(09), 14–24. <https://doi.org/10.18483/ijsci.2721>
51. Sparavigna, A. C. (2023). Asymmetric q-Gaussian functions to fit the Raman LO mode band in Silicon Carbide. ChemRxiv. Cambridge Open Engage; 2023.
52. Sparavigna, A. C. (2023). Generalizing asymmetric and pseudo-Voigt functions by means of q-Gaussian Tsallis functions to analyze the wings of Raman spectral bands. ChemRxiv, Cambridge Open Engage, 2023.
53. Sparavigna, A. C. (2023). Convolution and Fourier Transform: from Gaussian and Lorentzian Functions to q-Gaussian Tsallis Functions. International Journal of Sciences, 12(11), 7-11.
54. Sparavigna, A. C. (2024). Kubo Lineshape and its Fitted q-Gaussian Tsallis Function. International Journal of Sciences, 13(01), 1-9.
55. Stoneham, A. M. (1966). The theory of the strain broadened line shapes of spin resonance and optical zero phonon lines. Proceedings of the Physical Society, 89(4), 909.
56. Stoneham, A. M. (1969). Shapes of inhomogeneously broadened resonance lines in solids. Reviews of Modern Physics, 41(1), 82.
57. Stoneham, A. M. (1972). Linewidths with gaussian and lorentzian broadening. Journal of Physics D: Applied Physics, 5(3), 670.
58. Svelto, O. (1970). Principi dei laser. Tamburini editore.
59. Tagliaferro, A., Rovere, M., Padovano, E., Bartoli, M., & Giorelli, M. (2020). Introducing the novel mixed gaussian-lorentzian lineshape in the analysis of the raman signal of biochar. Nanomaterials, 10(9), 1748.
60. Tatum, J. (2022). Combination of Profiles. (2022, March 5). University of Victoria. <https://phys.libretexts.org/@go/page/6710>
61. Tennyson, Jonathan, Bernath, Peter F., Campargue, Alain, Császár, Attila G., Daumont, Ludovic, Gamache, Robert R., Hodges, Joseph T., Lisak, Daniel, Naumenko, Olga V., Rothman, Laurence S., Tran, Ha, Zobov, Nikolai F., Buldyreva, Jeanna, Boone, Chris D., De Vizia, Maria Domenica, Gianfrani, Livio, Hartmann, Jean-Michel, McPheat, Robert, Weidmann, Damien, Murray, Jonathan, Ngo, Ngoc Hoa and Polyansky, Oleg L.. "Recommended isolated-line profile for representing high-resolution spectroscopic transitions (IUPAC Technical Report)" Pure and Applied Chemistry, vol. 86, no. 12, 2014, pp. 1931-1943. <https://doi.org/10.1515/pac-2014-0208>
62. Thibault, F., Martinez, R. Z., Domenech, J. L., Bermejo, D., & Bouanich, J. P. (2002). Raman and infrared linewidths of CO in Ar. The Journal of chemical physics, 117(6), 2523-2531.
63. Tokmakoff, A. (2009). MIT Dept. of Chemistry, Lecture Notes, [Archive](#)
64. Townsend, R. (2008). Astronomy 310, Stellar Astrophysics, Fall Semester 2008, Lecture Notes, [Archive](#)
65. Tsallis, C. (1988). Possible generalization of Boltzmann-Gibbs statistics. Journal of statistical physics, 52, 479-487.
66. Tsallis, C. (1995). Some comments on Boltzmann-Gibbs statistical mechanics. Chaos, Solitons & Fractals, 6, 539-559.
67. Umarov, S., Tsallis, C., Steinberg, S. (2008). On a q-Central Limit Theorem Consistent with Nonextensive Statistical Mechanics. Milan J. Math. Birkhauser Verlag. 76: 307–328.
68. Yin, C., & Dong, H. (2023). The Bessel function expression of characteristic function. Communications in Statistics-Theory and Methods, 1-17.
69. Van Vleck, J. H. (1948). The dipolar broadening of magnetic resonance lines in crystals. Physical Review, 74(9), 1168.
70. Vogman, G. (2010). Deconvolution of spectral Voigt profiles using inverse methods and Fourier transforms. Department of Mathematics, University of Washington.